A Concentration-Time Hybrid Modulation Scheme for Molecular Communications

Mustafa Can Gursoy, Student Member, IEEE, Daewon Seo, Member, IEEE, and Urbashi Mitra, Fellow, IEEE

Abstract—Significant inter-symbol interference (ISI) challenges the achievement of reliable, high data-rate molecular communication via diffusion. In this paper, a hybrid modulation based on pulse position and concentration is proposed to mitigate ISI. By exploiting the time dimension, molecular concentration and position modulation (MCPM) increases the achievable data rate over conventional concentration and position-based modulations. In addition, unlike multi-molecule schemes, this hybrid scheme employs a single-molecule type and so simplifies transceiver implementations. In the paper, the optimal sequence detector of the proposed modulation is provided as well as a reduced complexity detector (two-stage, position-concentration detector, TPCD). A tractable cost function based on the TPCD detector is proposed and employed to optimize the design of the hybrid modulation scheme. In addition, the approximate probability of error for the MCPM-TPCD system is derived and is shown to be tight with respect to simulated performance. Numerically, MCPM shows improved performance over standard concentration and pulse position-based schemes in the low transmission power and high bit-rate regime. Furthermore, MCPM offers increased robustness against synchronization errors.

Index Terms—molecular communication via diffusion, modulation design, concentration-time modulation, hybrid modulation.

I. Introduction

Molecular communications is a promising bio-inspired communication for establishing nano-networks [2]. Among different ways of establishing molecular communication links, molecular communication via diffusion (MCD) has received particular attention due to its energy efficiency and biocompatibility [3]. In an MCD system, emitted molecules rely solely on free diffusion after emission from the transmitter to arrive at the receiver. Since the molecules propagate randomly in the environment, the arrival times at the receiver are random variables [4]. This physical phenomenon causes inter-symbol interference (ISI), which challenges reliable, high data-rate communication [5].

Modulation design remains an open problem in MCD systems due to the unique features of the communication channel. Standard approaches include encoding information in

- M. C. Gursoy and U. Mitra are with the Department of Electrical and Computer Engineering, University of Southern California, Los Angeles, CA 90089, USA (e-mails: {mgursoy, ubli}@usc.edu).
- D. Seo is with the Department of Electrical and Computer Engineering, University of Wisconsin-Madison, Madison, WI 53715, USA (e-mail: dseo24@wisc.edu).

This paper was presented in part at the IEEE International Conference on Communications (ICC 2020) [1]. This work has been funded in part by one or more of the following grants: ONR N00014-15-1-2550, NSF CCF-1817200, ARO W911NF1910269, Cisco Foundation 1980393, DOE DE-SC0021417, Swedish Research Council 2018-04359, NSF CCF-2008927, ONR 503400-78050.

the emission intensity (concentration shift keying, CSK, [6]), emitted molecule type (molecule shift keying, MoSK, [6], [7]), or emission time (pulse position modulation, PPM, [8]) of the molecular signal.

To combat ISI and increase data-rates, multiple molecule types have been employed to create orthogonal communication streams at the expense of more complex transceivers [9], [10]. Inhibitory molecules are employed in [11] to further reduce ISI, while in [12], [13], the molecule type is modified as a function of the past transmitted bits. Finally, multiple molecule types and PPM are the basis of the hybrid modulation in [14]. While these schemes achieve their goals, they rely on synthesizing, storing, and counting multiple types of molecules, thus incurring significantly increased complexity over a single-molecule method. Motivated by this, we consider emission timing as a degree of freedom coupled with single molecule type signaling herein.

As a timing-based modulation, PPM has received wide attention for radio-frequency based communications in ultra-wideband [15], visible light communications [16], etc. It has also been examined in the context of MCD [8], with maximum likelihood detection in the absence of ISI studied in [17] and higher order PPM for ISI mitigation investigated in [18].

In this paper, we encode information in emission concentration and time jointly. We observe that in an independent work [19], hybrid concentration-time modulation is also considered. Therein, the capacity of **ISI-free** concentration-time channels is examined and shown to be larger than that of concentration or time alone. We underscore that herein, we do consider ISI and there are trade-offs to be made in the **design** of the hybrid modulation in order to achieve the best BER performance in such channels. In our preliminary work [1], we had showed that the hybrid modulation scheme achieves lower BER than binary CSK (BCSK) and PPM in MCD channels with severe ISI. This paper extends and completes [1].

Overall, the key contributions of this paper are as follows:

- We propose a hybrid MCD modulation scheme that utilizes a single type of molecules. The proposed scheme merges K-PPM and BCSK, which we call K-ary molecular concentration and position modulation (K-MCPM).
- Considering the MCD channel faces ISI, we derive the maximum likelihood sequence detector (MLSD) for K-MCPM.
- In addition to the MLSD that is computationally expensive, we propose a two-stage, position-concentration detector (TPCD) that reduces complexity. TPCD first detects the emission time, then performs a fixed threshold (γ) to resolve the concentration information.

- The binary concentrations are characterized by a parameter $\alpha \in (0.5,1)$. The parameter α is optimized under the assumption of the use of TPCD and through the derivation of a convex proxy for the error probability. We also present a method that estimates the optimal threshold parameter γ .
- Our numerical results suggest that the theoretically optimized (α, γ) pair yields close-to-optimal performance compared to the values found via exhaustive search for TPCD.
- For a fixed (α, γ) pair, we derive the approximate error probability expression for a $\mathcal{K}\text{-MCPM}$ scheme.
- Our numerical results show that MCPM outperforms BCSK and PPM, especially when the bit-rate is high and the transmission power is low. Furthermore, our results show that the MCPM scheme is more robust to synchronization offsets than PPM scheme of the same order.

Our prior work [1] introduced the transmitter architecture of MCPM and the working principles of its TPCD detector. Herein, we complete these designs and analyses. In particular, we complete the modulation design by characterizing and solving the constellation point design problem for MCPM-TPCD. Furthermore, we derive the maximum likelihood sequence detector (MLSD) for MCPM, and introduce a low-complexity threshold selection method for TPCD. We also discuss the effects of temporal mis-synchronization on MCPM. Full derivations and proofs are provided herein in contrast to [1].

The rest of the paper is organized as follows: Section III introduces the channel model. Section III describes the proposed modulation scheme and discusses its key trade-off. Section IV introduces the optimal detector and a low complexity alternative which first detects position and then resolves the concentration. Section V derives the error probability of the MCPM-TPCD system. Section VI proposes theoretical methods to select the (α, γ) pair for an MCPM scheme. Section VII presents numerical error probability results. Lastly, Section VIII concludes the paper. Appendices A and B provide the proofs of the lemma and theorem presented in Section VI.

TABLE I LIST OF ABBREVIATIONS

Abbreviation	Full Name
BER	bit error ratio
BCSK	binary concentration shift keying
ES	exhaustive search
ISI	inter-symbol interference
LTI	linear time-invariant
MCD	molecular communication via diffusion
MCPM	molecular concentration and position modulation
ML	maximum likelihood
MLSD	maximum likelihood sequence detector
MoSK	molecule shift keying
PPM	pulse-position modulation
TPCD	two stage, position-concentration detector

II. SYSTEM MODEL

The MCD system in this paper involves a single point transmitter and a single spherical absorbing receiver of radius

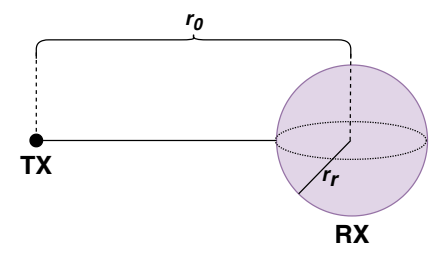


Fig. 1. The considered system model.

 r_r in an unbounded 3-D environment. The distance between the transmitter and the center of receiver is denoted by r_0 . The transmitter and the receiver are assumed to have perfect synchronization unless stated otherwise. A visualization of the propagation environment is provided in Figure 1. In this case, assuming that carrier molecules have a diffusion coefficient D, the arrival probability density of a molecule t seconds after its emission can be written as

$$f_{\text{hit}}(t) = \frac{r_r}{r_0 \sqrt{4\pi Dt}} \frac{1}{t} \frac{r_0 - r_r}{t} e^{-\frac{(r_0 - r_r)^2}{4Dt}},$$
 (1)

where $t \in (0, \infty)$.

In a time slotted channel with sequential transmissions, the MCD channel is characterized by the channel coefficients, where the n^{th} channel coefficient h_n can be computed as

$$h_n = \int_{(n-1)t_s}^{nt_s} f_{\text{hit}}(t)dt, \quad n = 1, 2, \dots, L.$$
 (2)

Here, t_s denotes the time within the receiver's counting intervals (*i.e.*, slots) and L is the considered channel memory. In reality, the considered channel has infinite memory due to the heavy right tail of the arrival distribution [20]. However, given that the arrival density function has small magnitude after a certain duration, we approximate the channel as having a finite duration, denoted by L. We select L by considering a total time after which we neglect the arrivals ($t_{\rm total}$), and computing L using $t_{\rm total}$ and t_s . Note that it is desirable to have a large $t_{\rm total}$ to satisfactorily capture the right tail of the arrival density function in Equation (1).

The channel coefficients h_n can be interpreted as a single molecule's probability of arrival at the receiver at the n^{th} slot after its release. In a time-slotted MCD system where multiple molecules are emitted for each transmitted symbol, we employ the linear time-invariant (LTI)-Poisson channel model to characterize the number of arriving molecules at each slot [21]. According to the LTI-Poisson model, the arrival count in the m^{th} time slot, denoted by R_m in this paper, is distributed as

$$R_m \sim \mathcal{P}\left(\sum_{n=1}^{L} N_{m-n+1} h_n\right),\tag{3}$$

where $\mathcal{P}(\cdot)$ denotes the Poisson distribution with argument as the rate parameter. In addition, N_m denotes the number of molecules emitted by transmitter at the beginning of the m^{th} time slot.

TABLE II		
AVERAGE EMITTED MOLECULES PER TRANSMISSION AND SLOT DURATIONS FOR BCSK.	PPM. AN	ND MCPM

Modulation Scheme	BCSK	2 -PPM	4 -PPM	8-PPM	2-MCPM	4-MCPM	8-MCPM	
Transmitted bits	1	1	2	2	2	2	1	
per unit symbol	1	1	۷	S	2	3	4	
Sub-intervals	1	2	4	8	2	4	Q	
per symbol	1		7	o	2	4		
Sub-interval duration (t_s)	t_b	$\frac{1}{2}t_b$	$\frac{2}{4}t_b$	$\frac{3}{8}t_b$	$\frac{2}{2}t_b = t_b$	$\frac{3}{4}t_b$	$\frac{4}{8}t_b$	
Bit duration	t_b	$\overline{t_b}$	t_b	t_b	t_b	t_b	t_b	
					BCSK bit-1	BCSK bit-1	BCSK bit-1	
Molecules per emission	2M for bit-1,	M $2M$	2M	3M	$2M \times 2\alpha$	$3M \times 2\alpha$	$4M \times 2\alpha$	
(N)	0 for bit-0		Z1VI		BCSK bit-0	BCSK bit-0	BCSK bit-0	
					$2M \times 2(1-\alpha)$	$3M \times 2(1-\alpha)$	$4M \times 2(1-\alpha)$	
Molecules per bit (on average)	M	M	M	M	M	M	M	

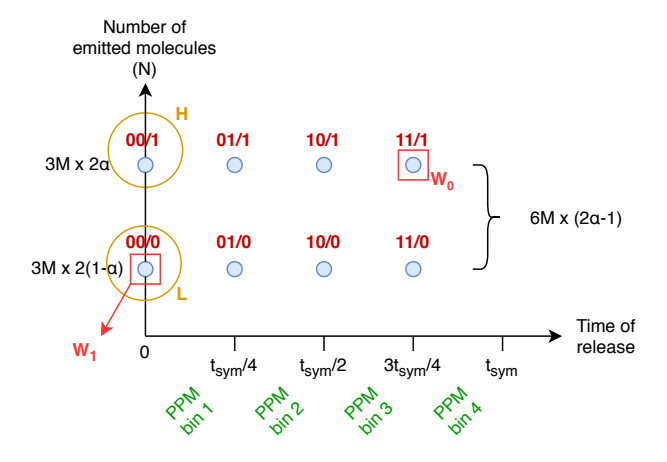


Fig. 2. The transmission strategy of 4-MCPM. The last bit determines the emission intensity of the molecular pulse, whereas the first two bits govern the emission instant. Circled constellation points are of interest in α optimization.

III. PROPOSED SCHEME

A. Modulation Description

Our proposed modulation scheme employs both concentration and the specific emission time of the molecules to convey information. Specifically, the proposed scheme combines the well-known PPM constellations with the conventional BCSK scheme and yields a two dimensional constellation diagram. Overall, the combination of \mathcal{K} -PPM and BCSK is referred to as the \mathcal{K} -ary molecular concentration-position modulation (\mathcal{K} -MCPM).

At the transmitter, a serial-to-parallel conversion is done to group the bit stream into groups of length $(\log_2 \mathcal{K}) + 1$ bits. As a convention, we consider the first $\log_2 \mathcal{K}$ to modulate the *PPM component* of the modulation whereas the last bit determines the *BCSK component*. In other words, the emission sub-interval of the molecular pulse is determined by the first $\log_2 \mathcal{K}$ bits, and the intensity of the said pulse is high or low depending on the BCSK bit being a "1" or "0". The transmission strategy for 4-MCPM is presented in Figure 2 for visualization purposes.

B. The Parameter α

Throughout the paper, the transmission power is normalized on a per bit basis [9], [18]. In an MCD system, the energy consumption is related to the number of emitted molecules [22]. Hence, the transmission power normalization is done through imposing an average number of emitted molecules (M) constraint. The value of M is a per-bit constraint such that each evaluated scheme emits, on average, M molecules per bit. Additionally, we also employ a bit-rate normalization by imposing a constant bit duration, t_b . Thus, as more bits are used per symbol, the symbol duration (t_{sym}) is longer.

For a \mathcal{K} -MCPM scheme, the symbol duration can be written as $t_{sym}=(1+\log_2\mathcal{K})t_b$, making each sub-slot duration $t_s=\frac{(1+\log_2\mathcal{K})t_b}{\mathcal{K}}$. Furthermore, for \mathcal{K} -MCPM, the average number of molecules emitted per \mathcal{K} -MCPM symbol is equal to $E[N]=(1+\log_2\mathcal{K})M$. Assuming all bits/symbols are equally likely, we have that

- the MCPM symbols having the BCSK bit '1' are transmitted with $N = 2\alpha(1 + \log_2 \mathcal{K})M$ molecules, and
- the MCPM symbols having the BCSK bit '0' are transmitted with $N = 2(1 \alpha)(1 + \log_2 \mathcal{K})M$ molecules,

where $\alpha \in (0.5,1)$. Table II is provided to show the implications of these constraints in MCPM, traditional BCSK, and PPM.

The α parameter defines the two concentration levels for the BCSK part of the hybrid constellation, and thus determines the distances between constellation points. The value of $\alpha=0.5$ results in no difference in concentration, yielding symbol ambiguities. On the other hand, if α is close to one, then the PPM signals for the BCSK symbols for the low concentration become hard to detect. Therefore, α is a design parameter to be optimized for an MCPM scheme. We formulate the α optimization problem in Section VI.

IV. RECEIVER DESIGN

A. Optimal Detector

Due to ISI, the maximum likelihood (ML) detectors for MCD modulations are in the form of ML sequence detectors (MLSD) [23]. We next present the MLSD for a \mathcal{K} -MCPM scheme herein.

Let $\mathcal S$ denote the block length in terms of MCPM symbols. In addition, we define $\lambda_{m|s}$ as the rate parameter of the arrival random variable at the m^{th} interval, conditioned on the MCPM symbol sequence s. Note that due to their definitions, $m \in \{1,\ldots,\mathcal S\mathcal K\}$ and s is a vector of length $\mathcal S$. Recalling the LTI-Poisson model in (3), $\lambda_{m|s}$ can be calculated as

$$\lambda_{m|s} = \sum_{n=1}^{\mathcal{K} \cdot L_s} N_{m-n+1|s} h_n \tag{4}$$

where $N_{m|s}$ denotes the number of emitted molecules by the transmitter at the m^{th} time slot, conditioned on the candidate symbol sequence s. Note that the rate parameter $\lambda_{m|s}$ depends on the transmitted symbol sequence as it follows from (3). By defining the vector $\mathbf{r} = \begin{bmatrix} R_1 & \dots & R_{\mathcal{S} \cdot \mathcal{K}} \end{bmatrix}$, the MLSD for a \mathcal{K} -MCPM scheme can be expressed as

$$\hat{\mathbf{s}} = \arg\max_{\mathbf{s}} P(\mathbf{r}|\mathbf{s})$$

$$= \arg\max_{\mathbf{s}} \prod_{m=1}^{S \cdot \mathcal{K}} \frac{\lambda_{m|\mathbf{s}}^{R_m} e^{-\lambda_{m|\mathbf{s}}}}{R_m!}$$

$$= \arg\max_{\mathbf{s}} \sum_{m=1}^{S \cdot \mathcal{K}} R_m \ln(\lambda_{m|\mathbf{s}}) - \lambda_{m|\mathbf{s}},$$
(5)

where \hat{s} denotes the vector of decoded symbols. For a block of length \mathcal{S} and a memory of L_s MCPM symbols (i.e., $L = \mathcal{K} \cdot L_s$), the \mathcal{K} -MCPM MLSD is of complexity $\mathcal{O}((2\mathcal{K})^{L_s}\mathcal{S})$ using a Viterbi decoder [24]. The MLSD is of high complexity, but will serve as a benchmark to illustrate the performance complexity trade-off for our proposed decoder introduced in the sequel.

B. A Reduced Complexity Detector

Herein, we present an MCPM detector with low complexity, which we call the two-stage, position-concentration detector (TPCD). It employs two stages as its name implies: One for the PPM information and another for the BCSK.

Recall that s_k represents the k^{th} MCPM symbol. At this point, we assume that $h_1 > \max(h_2, \ldots, h_L)$, which implies that the first path is dominant¹. Given this assumption, the intended sub-interval is expected to have the largest arrival count among the $\mathcal K$ PPM bins. Denoting the emission slot of s_k as q_k , the first stage of the detector performs

$$\hat{q}_k = \underset{j \in \{(k-1)\mathcal{K}+1,\dots,k\mathcal{K}\}}{\arg\max} R_j.$$
 (6)

Since arrival counts are Poisson random variables, the arrival count random variable with the largest expected value has the highest mean-over-standard deviation ratio. The second stage of the MCPM detector performs fixed threshold detection on the largest arrival count to detect the BCSK bit. Denoting the decision threshold as γ , the rule can be written as

$$R_{\hat{q}_k} \underset{H_0}{\overset{H_1}{\gtrless}} \gamma, \tag{7}$$

where H_0 and H_1 correspond to the hypotheses that the k^{th} MCPM symbol's BCSK bit being a '0' and a '1', respectively.

¹For MCD systems that yield practical error probabilities, this assumption is generally satisfied. However, it may not hold for extremely small symbol durations due to the behavior of (1).

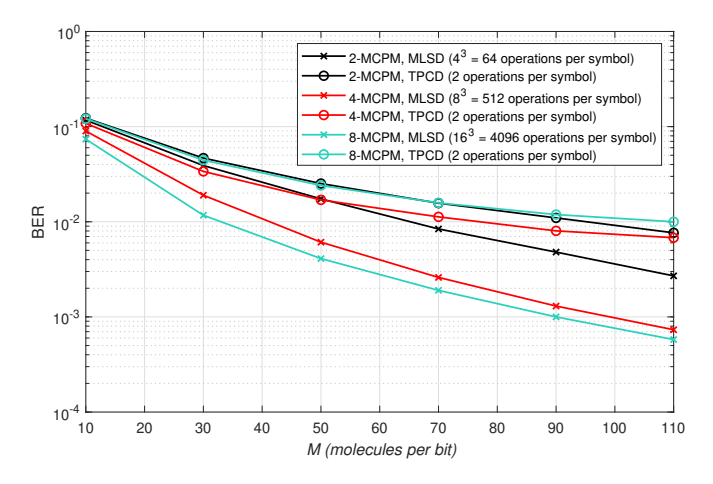


Fig. 3. BER vs. M curves for MCPM using MLSD and TPCD. $t_b=0.30\,\mathrm{s},$ $r_0=10\,\mathrm{\mu m},$ $r_r=5\,\mathrm{\mu m},$ $D=79.4\,\mathrm{\mu m}^2\,\mathrm{s}^{-1},$ $L_s=3.$ α and γ numerically optimized.

C. Comparing the Detectors

To compare the error performances of the two detection strategies, Figure 3 is presented. Note that a fixed and small symbol memory $L_s=3$ is selected for simulation, since the Viterbi decoding in the MLSD has exponential complexity in L_s .

As expected, the results of Figure 3 suggests that TPCD incurs a performance loss comparative to the optimal detector. Furthermore, it is observable that the performance gap increases with \mathcal{K} . Note that for a \mathcal{K} -MCPM scheme, TPCD only considers the largest of the \mathcal{K} obtained arrival counts, essentially disregarding the information coming from other $\mathcal{K}-1$ branches. On the other hand, the MLSD utilizes the arrival count information from all \mathcal{K} slots.

Since the Viterbi decoder performs $(2\mathcal{K})^{L_s}$ likelihood computations per each \mathcal{K} -MCPM symbol (*i.e.*, $\mathcal{O}((2\mathcal{K})^{L_s}\mathcal{S})$ per one block), it is considerably more complex than TPCD which performs only two comparisons ((6) and (7)) per symbol (*i.e.*, $\mathcal{O}(2\mathcal{S})$). This introduces a performance-complexity trade-off in terms of receiver design. In this paper, we will focus on the low-complexity option, TPCD, to demodulate MCPM symbols. Overall, the diagram of an MCD system that utilizes the MCPM scheme with TPCD is presented in Figure 4.

V. ERROR ANALYSIS

We have two design parameters which affect the performance of our overall system. To this end, we first provide an error analysis for the overall system given a fixed (α, γ) pair. Given the ISI characteristics of the MCD channel [1], [23], [25], the error probability can be found by averaging over conditional error probabilities. For a symbol memory of length L_s , this averaging is done over all possible symbol sequences of length L_s . Denoting the MCPM symbol sequence between the $(k-L_s+1)^{th}$ and k^{th} transmissions as $s_{k-L_s+1:k}$, we write

$$P_e = \sum_{\forall s_{k-L_s+1:k}} \left(\frac{1}{2\mathcal{K}}\right)^{L_s} P_{e|s_{k-L_s+1:k}}.$$
 (8)

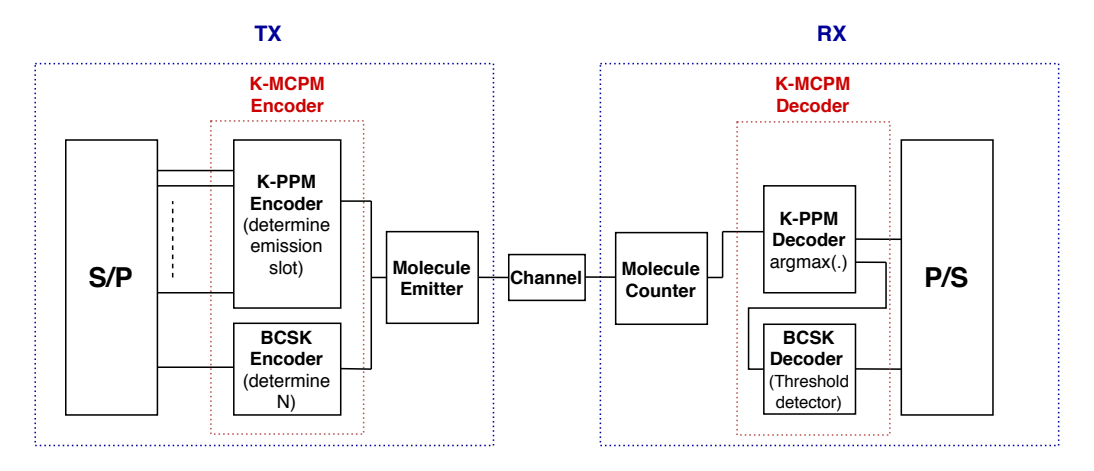


Fig. 4. Overall transmission and reception model of an MCD system utilizing $\mathcal{K} ext{-MCPM}$ and the TPCD.

Denoting $d_H(\cdot,\cdot)$ as the Hamming distance operator, we proceed by obtaining the conditional error probability expression on the right-hand side as

$$P_{e|s_{k-L_s+1:k}} = \sum_{n=1}^{2\mathcal{K}} \frac{d_H(\mathbf{v}_{s_k}, \mathbf{v}_n)}{1 + \log_2 \mathcal{K}} P(\hat{s}_k = n | s_{k-L_s+1:k}).$$
 (9)

Here, $\mathbf{v}_{(\cdot)}$ denotes the binary vector corresponding to the integer symbol in its argument, and \hat{s}_k denotes the detected symbol.

From (9), we seek to characterize $P(\hat{s}_k = n | s_{k-L_s+1:k})$. Denoting the conditional event $\{\hat{s}_k = n | s_{k-L_s+1:k}\}$ as \hat{n} , we note that the expression for $P(\hat{n})$ depends on the BCSK constellation of the intended bit. Let $b_m \in \{b_1, \ldots, b_{\mathcal{K}}\}$ be the corresponding integer representation of the PPM bins of the MCPM symbol determined by \mathbf{v}_n . Therefore, R_{b_m} is a random variable conditioned on the $s_{k-L_s+1:k}$ sequence that describes the arrival count of $R_{(k-1)\mathcal{K}+m}$. $P(\hat{n})$ can be written as

$$P(\hat{n}) = \begin{cases} P(R_{b_m} > \max(R'_{b_m}), R_{b_m} > \gamma) & \text{if } v_n[1 + \log_2 \mathcal{K}] = 1, \\ P(R_{b_m} > \max(R'_{b_m}), R_{b_m} \le \gamma) & \text{if } v_n[1 + \log_2 \mathcal{K}] = 0, \end{cases}$$
(10)

where R'_{b_m} denotes the set of arrival counts corresponding to each bin other than b_m . Denoting $Y = \max(R'_{b_m})$, we can find $P(\hat{n})$ where $v_n[1 + \log_2 \mathcal{K}] = 0$ as

$$P(R_{b_m} > \max(R'_{b_m}), R_{b_m} \leq \gamma) = P(Y < R_{b_m} \leq \gamma)$$

$$= \int_{-\infty}^{\gamma} \left[\int_{y}^{\gamma} f_{R_{b_m}}(r) dr \right] f_Y(y) dy$$

$$= \int_{-\infty}^{\gamma} \left[\int_{-\infty}^{r} f_Y(y) dy \right] f_{R_{b_m}}(r) dr$$

$$= \int_{-\infty}^{\gamma} F_Y(r) f_{R_{b_m}}(r) dr.$$
(11)

Using the Gaussian approximation on the Poisson arrival

counts [26], the CDF of Y can be found as

$$F_{Y}(r) = P\left(\max(R'_{b_{m}}) \le r\right)$$

$$= \prod_{\substack{\tau=1\\ \tau \neq b_{m}}}^{\mathcal{K}} P(R_{b_{\tau}} \le r)$$

$$= \prod_{\substack{\tau=1\\ \tau \neq b_{m}}}^{\mathcal{K}} \left[1 - Q\left(\frac{r - \mu_{R_{b_{\tau}}}}{\sigma_{R_{b_{\tau}}}}\right)\right],$$
(12)

where $Q(\cdot)$ is the complementary cumulative distribution function of the standard Gaussian. Here, $\sigma_{Rb_{\tau}} = \sqrt{\mu_{Rb_{\tau}}}$ as the arrival counts are Poisson random variables. In addition, each mean (rate) parameter conditioned on $s_{k-L_s+1:k}$ can be found as $\mu_{Rb_{\tau}} = \sum_{n=1}^{\mathcal{K}\cdot L_s-1} N_{(k-1)\mathcal{K}+\tau-n+1}h_n$, due to the LTI-Poisson nature of the channel as described in (3). We also note that the non-zero N values (i.e., emitted number of molecules at transmission instants) are either $B\alpha$ or $B(1-\alpha)$ depending on the concentration constellation, where $B=2M(1+\log_2\mathcal{K})$. Lastly, Similar to (11), $P(\hat{n})$ for the case where $v_n[1+\log_2\mathcal{K}]=1$ can be expressed as

$$P(R_{b_m} > \max(R'_{b_m}), R_{b_m} > \gamma) = \int_{\gamma}^{\infty} F_Y(r) f_{R_{b_m}}(r) dr,$$
(13)

completing our derivation.

Figure 5 provides the probability of error versus M for different MCPM orders to demonstrate the accuracy of Equations (8)-(12). Furthermore, Figure 6 presents BER versus t_b to evaluate the accuracy of the derived BER under different ISI magnitudes. While, our probability of error derivation invokes approximations, Figures 5 and 6 confirm that the closed form expressions provide good approximations to the true probability of error.

VI. THE OPTIMIZATION OF α AND γ

As noted in Section III, for a fixed M, α is a parameter that poses a trade-off between the detection accuracies of the position and concentration constellations. For an MCPM system that uses TPCD at the receiver, we see that the (α, γ) pair needs

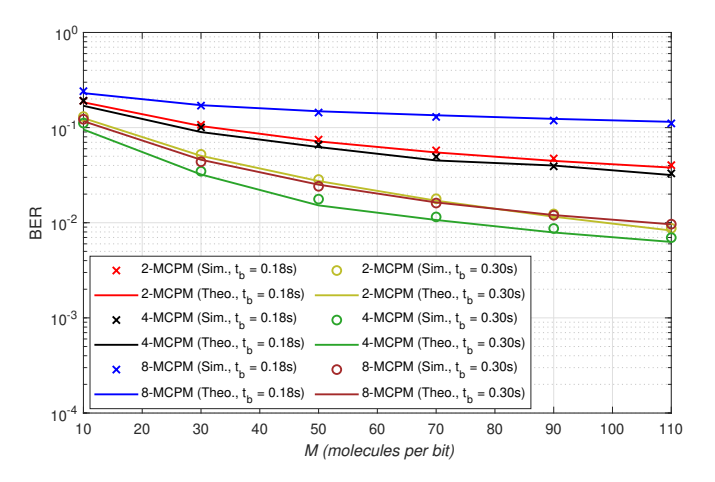


Fig. 5. BER vs. M curves. $t_b=0.18$ and 0.30s, $r_0=10\mu\text{m}, r_r=5\mu\text{m},$ $D=79.4\frac{\mu m^2}{s}$, and $t_{\text{total}}=12t_b$. (α,γ) pairs optimized through exhaustive search.

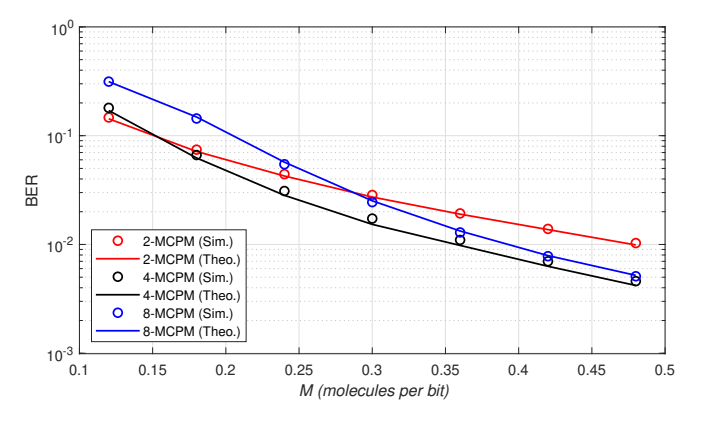


Fig. 6. BER vs. t_b curves. M=50 molecules, $r_0=10\mu\text{m}$, $r_r=5\mu\text{m}$, $D=79.4\frac{\mu m^2}{s}$, and $t_{\text{total}}=12t_b$. (α,γ) pairs optimized through exhaustive search

to be optimized with the goal of minimizing the probability of error. In this section, we address this optimization problem.

Directly optimizing the probability of error expression derived in Equations (8)-(13) is computationally expensive as one would need to consider $(2\mathcal{K})^{L_s}$ conditional error probabilities for each evaluated (α,γ) pair. To this end, we determine methods informed by the true probability of error and take a two-step approach: We first estimate α and then use the estimated α to optimize γ .

A. Selecting α

Herein, inspired by the properties of an MCPM scheme and the nature of the MCD channel, we propose a low-complexity sub-optimal cost function that is provably convex under reasonable conditions. Note that α determines the distances between different MCPM constellation points. For tractability, when optimizing α , we use a hypothetical no-ISI scenario (even though the evaluated channel has ISI) instead of considering the ISI between consecutive MCPM symbols. Our results will show that this approximation is not detrimental to overall performance.

The no-ISI assumption corresponds to the case where the channel is cleared after each MCPM symbol. Note that the ISI is still present within the temporal bins of each MCPM symbol. In this hypothetical scenario, among each column of the 2-D constellation diagram, the left-most one is the most likely to be detected erroneously. Therefore, we focus our design into the left-most constellation points (*i.e.*, the circled points "H" and "L" in Figure 2).

The error probabilities associated with these points can be written as

$$\begin{split} P_{e|H} &= P(R_1 < R_2 \cup \dots \cup R_1 < R_{\mathcal{K}} \cup R_1 < \gamma | \text{H sent}) \\ P_{e|L} &= P(R_1 < R_2 \cup \dots \cup R_1 < R_{\mathcal{K}} \cup R_1 > \gamma | \text{L sent}). \end{split} \tag{14}$$

We use the union bound on the expression $P_{e|H} + P_{e|L}$ to determine our cost function as

$$C = P(R_1 < \gamma | \text{H sent}) + P(R_1 > \gamma | \text{L sent})$$

$$+ \sum_{i=2}^{K} P(R_1 < R_i | \text{H sent}) + P(R_1 < R_i | \text{L sent}).$$
(15)

Using the Gaussian approximation on the arrival counts [26], we obtain

$$C = Q\left(\frac{B\alpha_U h_1 - \gamma_U}{\sqrt{B\alpha_U h_1}}\right) + Q\left(\frac{\gamma_U - B(1 - \alpha_U)h_1}{\sqrt{B(1 - \alpha)h_1}}\right) + \sum_{i=2}^{K} Q\left(\frac{B\alpha_U (h_1 - h_i)}{\sqrt{B\alpha_U (h_1 + h_i)}}\right) + Q\left(\frac{B(1 - \alpha_U)(h_1 - h_i)}{\sqrt{B(1 - \alpha_U)(h_1 + h_i)}}\right),$$
(16)

where the (α_U, γ_U) pair represents the α and γ values for the hypothetical no-ISI scenario.

Minimizing C requires the optimization of α_U and γ_U jointly. However, by deriving the optimal γ_U value in terms of α_U , we can reduce the dimension of the numerical search. We now show the convexity of C in α_U under the following set of conditions:

$$0.5 < \alpha_{U} < 1$$

$$B(1 - \alpha_{U})h_{1} < \gamma_{U} < B\alpha_{U}h_{1}$$

$$h_{1} > \max(h_{2}, \dots, h_{K}) > 0$$

$$B\alpha h_{1} - B(1 - \alpha)h_{1} > 3$$
(17)

Note that the first two conditions define the valid intervals of the parameters α_U and γ_U . Here, the interval of α_U follows from the definition of the parameter in Subsection III-B, and γ_U needs to lie within the interval $(B(1-\alpha_U)h_1, B\alpha_Uh_1)$ to be a meaningful threshold. The third condition assumes that the symbol duration is defined such that the first channel coefficient is the largest one. The last condition lower bounds the distance between the expected arrival counts of adjacent concentration constellations and is typically satisfied in practical MCD links, including all data points generated in the paper.

We first start by finding the optimal γ_U for each α_U that minimizes C by providing the following lemma:

Lemma 1 (Convexity in γ_U). For all $\alpha_U \in (0.5, 1)$, the cost function C is convex in γ_U , given the validity condition $B(1 - \alpha_U)h_1 < \gamma_U < B\alpha_Uh_1$ is held.

Proof. The proof is provided in Appendix A.

Given Lemma 1, the optimal γ_U can be found from the vanishing point of $\frac{\partial C}{\partial \gamma_U}$, written as

$$\gamma_U^*(\alpha_U) = \sqrt{\frac{Bh_1 + \ln(\frac{1 - \alpha_U}{\alpha_U}) - 2B\alpha_U h_1}{\frac{1}{B\alpha_U(1 - \alpha_U)h_1} - \frac{2}{B(1 - \alpha)h_1}}}.$$
 (18)

Given that we now have an expression of the optimal γ_U for each α_U , we can now show that C is convex in α_U when $\gamma_U = \gamma_U^*(\alpha_U)$.

Theorem 1 (Convexity in α_U). Given that the conditions in (17) is met, C is convex in α_U when $\gamma_U = \gamma_U^*(\alpha_U)$.

Proof. The proof of Theorem 1 is given in Appendix B.

At this point, for the no-ISI scenario, we have found γ_U^* in closed form as a function of α_U , and shown the union bound cost function C to be convex in α_U when operating at $\gamma_U = \gamma_U^*(\alpha_U)$. Therefore, C can be minimized using simple 1-dimensional numerical search algorithms, and α^* can be found. Note that performing this operation only once (before the data transmission starts) is sufficient. It is also noteworthy that γ_U is simply a dummy variable in this derivation. The obtained α^* is employed to determine γ in the following.

B. Selecting γ

In Subsection VI-A, a hypothetical no-ISI scenario is considered to optimize α . However, the same approach cannot be taken for γ , since completely ignoring earlier symbol transmissions causes the obtained γ to be considerably smaller than the actual optimal value. Motivated by this shortcoming, we propose a low complexity, sub-optimal method for estimating the γ value in the actual, with-ISI scenario. The proposed approach works as follows:

- 1) The *worst-case symbol sequences* for each point on the constellation diagram in terms of ISI are considered.
 - For the MCPM constellation points where the concentration bit is a 0 (*i.e.*, the bottom row), the worst-case sequence is the one causing the highest ISI. The highest ISI is generated when all the past symbols are transmitted at the \mathcal{K}^{th} sub-slot and with the high concentration. For a symbol memory of L_s and using 4-MCPM, this sequence corresponds to a (L_s-1) symbols-long repeated transmission of W_0 in Figure 2. Note that this is similar to the "...-1-1-1-1-1-0" case in pure BCSK.
 - Similarly, for the MCPM constellation points where the concentration bit is a 1 (top row), the worst-case sequence is the one causing the lowest ISI, since ISI would *help* the correct detection of the concentration bit otherwise [27]. For a symbol memory consideration of L_s and using 4-MCPM, this sequence corresponds to a (L_s-1) symbols-long repeated transmission of W_1 in Figure 2. Note that this is similar to the "...-0-0-0-0-0-1" case in pure BCSK.

Let $\mu^w_{i,j}$ be the conditional arrival mean of the constellation point located at the i^{th} PPM bin and has

the BCSK bit j, under the corresponding worst-case sequence considerations. Here, $i \in \{1, ..., \mathcal{K}\}$ and $j \in \{0, 1\}$. These conditional arrival means can be written as

$$\mu_{i,j}^{w} = \begin{cases} B\alpha^* h_1 + \sum_{c=1}^{L_s - 1} B(1 - \alpha^*) h_{c\mathcal{K} + i} & j = 1, \\ B(1 - \alpha^*) h_1 + \sum_{c=1}^{L_s - 1} B\alpha^* h_{(c-1)\mathcal{K} + i + 1} & j = 0. \end{cases}$$
(19)

2) After finding the conditional statistics, the Gaussian approximation of the Poisson distribution is again employed, in order to find an individual threshold between the upper and lower-row constellations of the i^{th} PPM bin, which we call γ_i^w . Specifically, γ_i^w locates at the point where the upper ($\sim \mathcal{N}(\mu_{i,1}^w, \mu_{i,1}^w)$) and lower ($\sim \mathcal{N}(\mu_{i,0}^w, \mu_{i,0}^w)$) constellations' densities intersect. Thus, γ_i^w is the solution to the equation

$$\frac{1}{\sqrt{2\pi\mu_{i,1}^{w}}}e^{\frac{(\gamma_{i}^{w}-\mu_{i,1}^{w})^{2}}{2\mu_{i,1}^{w}}} = \frac{1}{\sqrt{2\pi\mu_{i,0}^{w}}}e^{\frac{(\gamma_{i}^{w}-\mu_{i,0}^{w})^{2}}{2\mu_{i,0}^{w}}}.$$
 (20)

3) Lastly, the obtained candidate γ_i^w values are averaged to find the estimated γ as

$$\gamma^* = \left| \frac{1}{\mathcal{K}} \sum_{i=1}^{\mathcal{K}} \gamma_i^w \right| + \frac{1}{2}. \tag{21}$$

The floor function operation in (21) is done since in the actual case, the arrival counts are discrete and Poisson distributed random variables.

VII. NUMERICAL RESULTS

Herein, numerical BER results of the proposed scheme are presented under different channel conditions and detectors through computer simulations, on the LTI-Poisson channel model described in Section II,² and using the parameters as presented in Table III.³ Since MCPM is a combination of BCSK and \mathcal{K} -ary PPM, the proposed scheme is compared to these modulation schemes in order to present the gain it has over its building blocks. In addition, unless specified, all (α, γ) pairs of the MCPM schemes in the section are obtained via exhaustive search and using TPCD, and thus presumed to be the optimal values. BCSK is demodulated using a numerically optimized threshold detector similar to Equation (7), and PPM schemes are demodulated using the maximum count decoder similar to Equation (6). All figures herein employ the normalizations presented in Table II.

A. Performance Evaluation of the α and γ Optimizations

Both α and γ selection methods are sub-optimal procedures due to their simplifying considerations. Thus, this subsection provides numerical results regarding the accuracy of the proposed methods to select the (α, γ) pair. Figure 7 presents the theoretical and optimal (α, γ) pairs for a set of

²Note that in both Equation (6) and α optimization, we had assumed $h_1 > \max(h_2,\dots,h_L)$. Though it is generally satisfied, this assumption is not imposed on any evaluated system in this paper. The channel coefficients are generated using Equations (1)-(2), according to the system parameters.

 3 The chosen value for D is reported to be a conservative value for the diffusion coefficient of insulin in water at 20°C [28].

TABLE III

CONSIDERED SYSTEM AND CHANNEL PARAMETERS. DEFAULT VALUES
SHOWN IN BOLD.

Parameter	Value
M (molecules)	10, 30, 50 , 70, 90, 110
t_b (s)	0.12, 0.18, 0.24, 0.30 , 0.36, 0.42, 0.48
$r_0 \; (\mu \mathrm{m})$	10
r_r (μm)	5
$D (\mu \text{m}^2 \text{s}^{-1})$	79.4

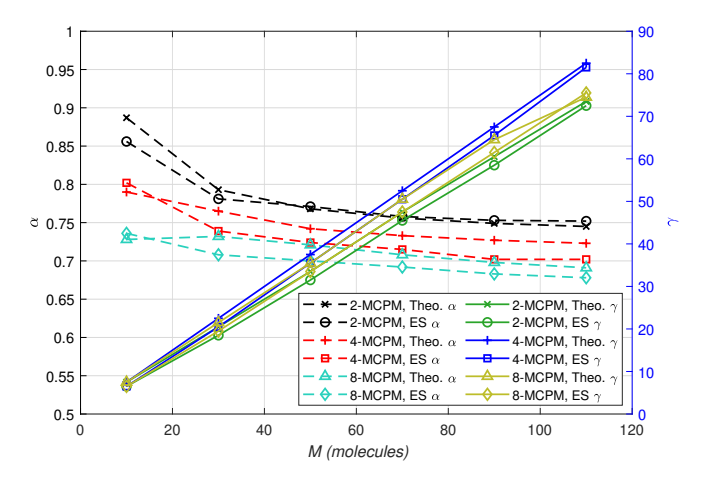


Fig. 7. α and γ vs. M for MCPM, using theoretical and simulated values. $t_b=0.30\,\mathrm{s}, r_0=10\,\mathrm{\mu m}, r_r=5\,\mathrm{\mu m}, D=79.4\,\mathrm{\mu m}^2\,\mathrm{s}^{-1},$ and $t_{\mathrm{total}}=48t_b$.

channel parameters. Throughout the subsection, the theoretical curves correspond to calculating both α and γ using methods described in Section VI, whereas the curves using true optimal values use (α, γ) pairs are calculated using exhaustive search (ES).

Overall, the results of Figure 7 suggest that the results of our optimizations follow the trends of the true (α, γ) pairs. That being said, the effect of the slight discrepancies need to be addressed to assess the sensitivity of the error performance with respect to α and γ . In order to evaluate the error performance achieved by the optimization approaches presented in Subsections VI-A and VI-B, two sets of results are presented. Firstly, Figure 8 is presented to evaluate the performance with respect to M, using the (α, γ) pairs obtained for Figure 7. In addition, Figure 9 is presented to evaluate the effect of t_b on the performance.

The numerical results of Figures 8 and 9 suggest that the BER obtained by employing the (α, γ) pairs found via our optimization strategies closely approximate the BER obtained through numerical exhaustive searched (α, γ) pairs. Note that Figure 9 shows that our method is especially effective when the bit duration t_b is smaller, which is desirable as the high bit-rate regime is indeed our operation regime of interest. That being said, a slight performance loss is incurred at larger t_b values (lower data-rate).

Our empirical observations suggest that the accuracy in estimating the optimal α does not considerably increase in the absolute error sense as t_b increases. However, we observed that the sensitivity of the error performance to α increases with t_b , which partially causes the slight performance loss incurred by the sub-optimal methods. One interesting finding is that

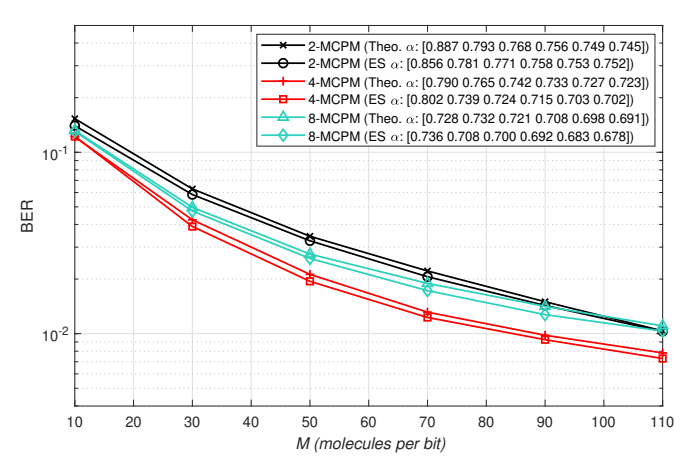


Fig. 8. BER vs. M curves for MCPM. $t_b=0.30~{\rm s},$ $r_0=10~{\rm \mu m},$ $r_r=5~{\rm \mu m},$ $D=79.4~{\rm \mu m}^2~{\rm s}^{-1},$ and $t_{\rm total}=48t_b.$

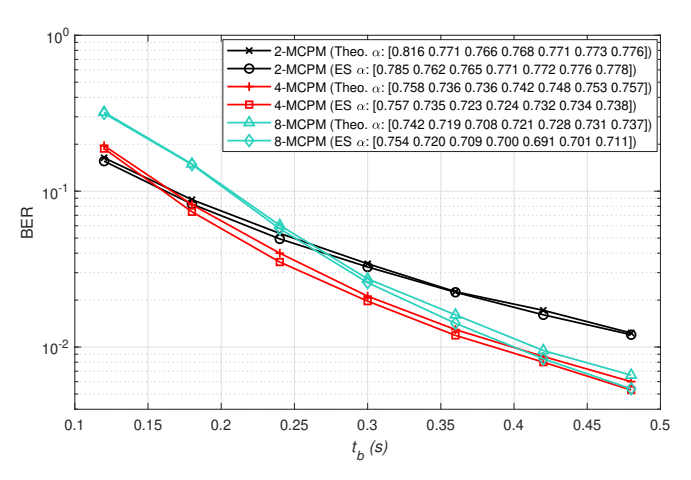


Fig. 9. BER vs. t_b curves for MCPM. M=50 molecules, $r_0=10\,\mu\text{m}$, $r_r=5\,\mu\text{m}$, $D=79.4\,\mu\text{m}^2\,\text{s}^{-1}$, and $t_{\text{total}}=48t_b$.

even though a larger t_b implies the accuracy of the no-ISI assumption to improve, the absolute error between the optimal and estimated α does not monotonically decrease with t_b . This behavior is due to the sub-optimality introduced in the union bound in Equation (15), as the bounding results in counting some decision regions multiple times [29].

In addition to the aforementioned discussion, a portion of the performance gap can be explained due to the approximations done in the γ optimization. As t_b increases, the incurred ISI decreases for all symbol sequences, including the worst-case sequences for the MCPM scheme. This, in turn, decreases the ISI contribution of conditional arrival statistics. In fact, this decrease leads some candidate γ_i^w values to undershoot, causing the obtained γ^* from Equation (21) to be smaller than the actual value. Overall, emphasizing on the goals of establishing high data-rate communication (small t_b) with low power consumption (small M) and low computational complexity, we believe that despite their shortcomings in the large t_b regime, the proposed sub-optimal methods for determining α and γ still have utility in the regime of interest.

B. Error Performance and Transmission Power

In a nano-scale MCD link, energy consumption is an important design criterion. Acknowledging the presence of the relation between the consumed energy and the number of emitted molecules [22], this subsection presents the error performance of MCPM with respect to M. Here, Figure 10 considers a high ISI scenario given the channel parameters, whereas Figure 11 has a more benign channel.

The results of Figure 10 suggest that under high ISI, the proposed scheme outperforms its concentration and position counterparts. The main reason for this desirable gain is the ability of MCPM to encode more bits within its constellations, effectively mitigating ISI by having a longer symbol duration while still satisfying the same bit-rate constraint $(\frac{1}{t})$. One interesting observation is that when using the TPCD, although increasing K corresponds to having a sparser transmission in the temporal axis, the error performance of K-MCPM does not monotonically improve with K. We note this phenomenon is present despite the fact that higher K also allows emissions with larger numbers of molecules (see Table II). Since ISI is considerably high in Figure 10, further dividing the already short symbol duration into a large number of temporal subslots exacerbates the ISI issue between them. Thus, it can be inferred that the MCPM order K inherently governs a tradeoff between the observed ISI and the transmission (hence also received) power. Overall, given the considered system parameter set, 4-MCPM is found to yield the lowest error probabilities among the evaluated schemes.

The results of Figure 11 suggest that MCPM still has an error performance improvement in the milder ISI regime, though the gain is less pronounced than the higher bit-rate scenario in Figure 10. It can also be observed that as M increases, pure PPM starts to become the more desirable choice than the proposed scheme, whilst in the lower transmission power range (small M), MCPM schemes outperform BCSK and PPM. Since MCPM schemes can encode more bits in a single symbol, they can emit more molecules for each symbol under the M normalization, as also presented in Table II. This property is especially beneficial when M is smaller, as it helps MCPM schemes avoid extremely low emission intensities better than its competitors in this regime.

C. Error Performance and Bit-Rate

The results and discussion presented in Subsection VII-B suggest that MCPM compares to its concentration and position components differently under different amounts of ISI. Since the ISI in an MCD system depends on the relationship between the topological parameters and the symbol duration, Figure 12 is presented to evaluate the error performance of MCPM with respect to t_b .

The results of Figure 12 show that even though pure PPM is a better strategy for larger t_b scenarios, at least one order of MCPM outperforms the existing schemes in high bit-rate scenarios. Combined with the results presented in Subsection VII-B, MCPM is found to be especially beneficial when the bit-rate is relatively high (small t_b) and the transmission power is relatively low (small M), which suggests possible

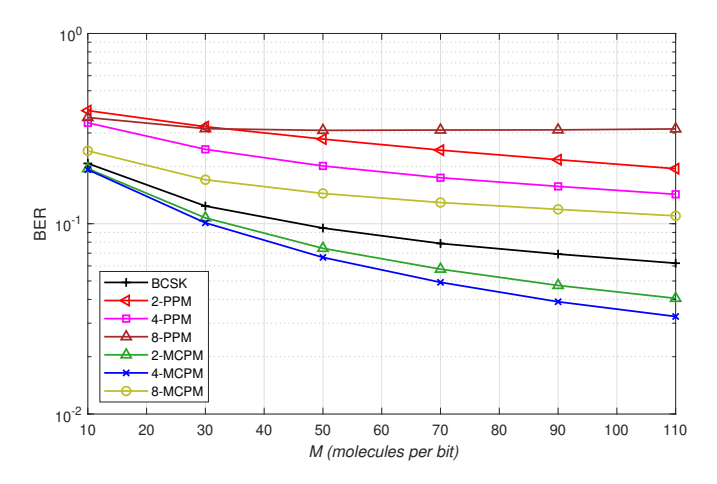


Fig. 10. BER vs. M curves for MCPM and competing schemes. $t_b=0.18\,\mathrm{s}$, $r_0=10\,\mathrm{\mu m},\,r_r=5\,\mathrm{\mu m},\,D=79.4\,\mathrm{\mu m^2\,s^{-1}},\,\mathrm{and}\,\,t_{\mathrm{total}}=48t_b.$

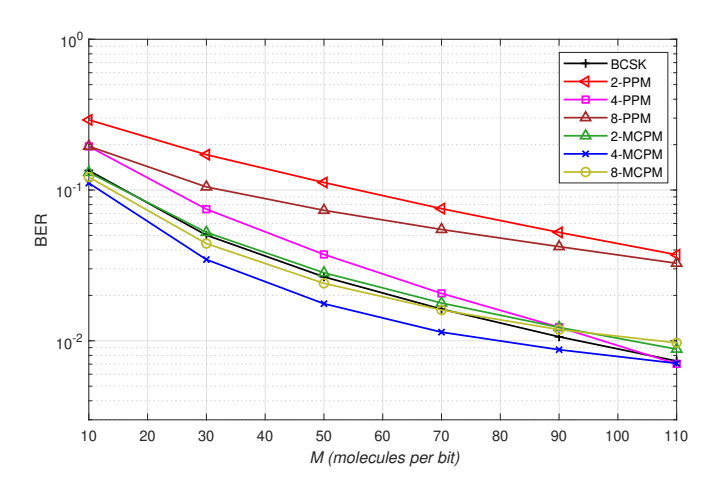


Fig. 11. BER vs. M curves for MCPM and competing schemes. $t_b=0.30\,\mathrm{s},$ $r_0=10\,\mathrm{\mu m},\,r_r=5\,\mathrm{\mu m},\,D=79.4\,\mathrm{\mu m^2\,s^{-1}},\,\mathrm{and}\,\,t_{\mathrm{total}}=48t_b.$

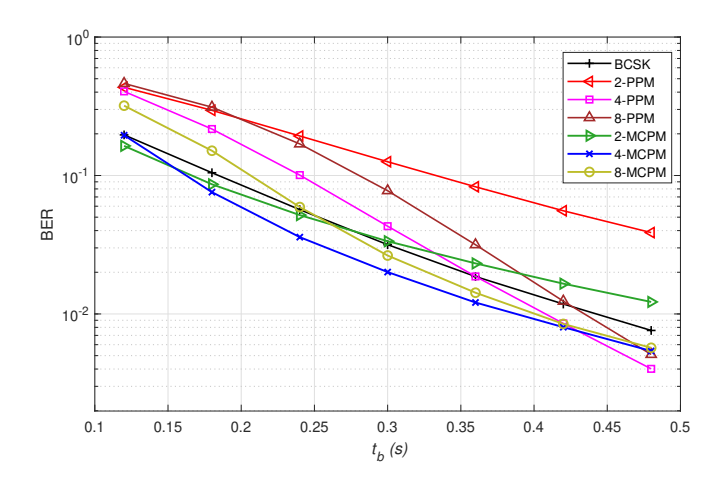


Fig. 12. BER vs. t_b curves for MCPM and competing schemes. M=50 molecules, $r_0=10\,\mu\text{m},\,r_r=5\,\mu\text{m},\,D=79.4\,\mu\text{m}^2\,\text{s}^{-1}$, and $t_{\text{total}}=30\,\text{s}$.

applications for MCD under these channel conditions and with simple nano-scale machinery. Furthermore, noting that the results presented in Figures 8-9 suggest the proposed α and γ selection techniques are accurate in the mentioned regime, it follows that within the parameter regimes where MCPM is

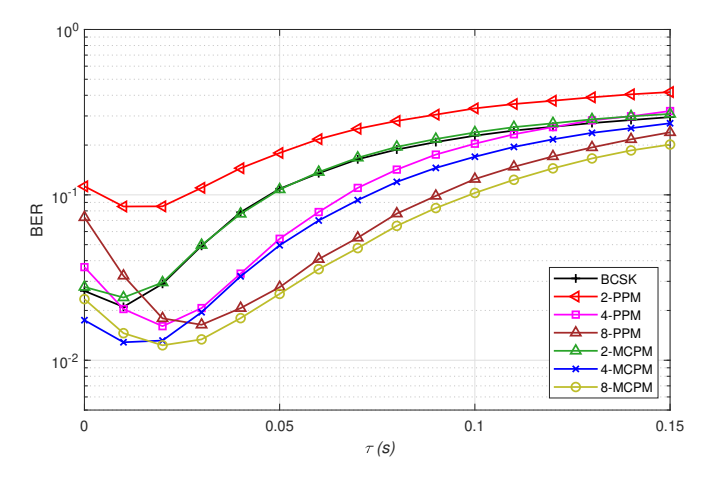


Fig. 13. BER vs. τ curves for MCPM and competing schemes. M=50 molecules, $t_b=0.30\,\mathrm{s},\ r_0=10\,\mathrm{\mu m},\ r_r=5\,\mathrm{\mu m},\ D=79.4\,\mathrm{\mu m}^2\,\mathrm{s}^{-1},\ t_{\mathrm{total}}=48t_b.$

beneficial, the presented numerical results for MCPM can be closely approximated using the proposed methods.

D. Error Performance under Imperfect Synchronization

Although perfect synchronization between the transmitter and the receiver was assumed until this point, this assumption may not always hold in an MCD link [30]. In this section, the robustness and general behavior of MCPM under missynchronization are investigated. Specifically, the scenario in which the receiver's clock lags behind the transmitter's clock is examined, where the parameter τ denotes the clock offset between them. The (α, γ) pairs for the MCPM schemes, alongside the threshold values for BCSK are numerically optimized for each τ . Using these definitions and considerations, Figure 13 presents the obtained BER versus τ curves.

The results of Figure 13 imply that in the very high τ regime (large synchronization error), the MCPM and PPM schemes with higher orders outperform their lower order counterparts. This phenomenon is mainly due to allowing a larger symbol duration while still satisfying the same t_b constraint, since having a larger t_{sym} makes τ smaller with respect to the symbol duration. This effect also explains the phenomenon of MCPM outperforming pure PPM with the same order, since the concentration dimension allows to encode more bits into a single symbol than pure PPM.

An interesting observation in Figure 13 is that the error performance does monotonically deteriorate as τ increases. This phenomenon has been documented in the literature for BCSK, in the context of deliberately adding a reception delay to improve error performance [31]. The results of Figure 13 suggest that the BER improvement introduced by a reception delay is also applicable to timing-based modulation schemes like MCPM and PPM as well. The main reason for this beneficial phenomenon is linked to the behavior of the arrival time distribution. There is a non-negligible delay between the emission instant and the channel peak time [20], which implies that within this time interval, ISI contributes to the received signal more than the intended symbol does. Having a τ delay in the reception window can help the receiver to mitigate ISI

(at the cost of reducing the received signal power) and be beneficial. Of course, further increasing τ causes losing the intended symbol's contribution as well, resulting in a poorer error performance.

VIII. CONCLUSIONS

In this paper, the problem of MCD modulation design using a single type of molecules has been addressed. To this end, a hybrid modulation scheme, molecular concentration position modulation (MCPM), has been proposed. The MLSD for the proposed modulation has been derived. Motivated by the high computational complexity of MLSD, a reduced complexity sub-optimal detector (i.e., TPCD) has been introduced. For an MCPM scheme utilizing TPCD, the problem of constellation point design has been addressed through the parameter α . In order to optimize α , a cost function has been proposed and was shown to be convex in α . Furthermore, a low-complexity sub-optimal strategy to select the threshold used in TPCD was presented. Overall, our numerical results suggest that MCPM schemes outperform BCSK and PPM especially in the high bit-rate and low transmission power regime, and provide better robustness against synchronization errors between the transmitter and the receiver.

APPENDIX A PROOF OF LEMMA 1

The proof simply follows from showing that $\frac{\partial^2 C}{\partial \gamma_U^2} > 0$ holds within the valid region. The second derivative is found as

$$\frac{\partial^{2} C}{\partial \gamma_{U}^{2}} = \frac{1}{\sqrt{2\pi}} \left(\frac{\gamma_{U} - B(1 - \alpha_{U})h_{1}}{(B(1 - \alpha_{U})h_{1})^{3/2}} e^{-\frac{(\gamma_{U} - B(1 - \alpha_{U})h_{1})^{2}}{2B(1 - \alpha_{U})h_{1}}} - \frac{\gamma_{U} - B\alpha_{U}h_{1}}{(B\alpha_{U}h_{1})^{3/2}} e^{-\frac{(\gamma_{U} - B\alpha_{U}h_{1})^{2}}{2B\alpha_{U}h_{1}}} \right).$$
(22)

Note that the exponential expressions are always positive, $(B\alpha_U h_1)$ and $B(1-\alpha_U)h_1$ are positive by definition, $\gamma_U-B(1-\alpha_U)h_1$ is positive and $\gamma_U-B\alpha_U h_1$ is negative due to the defined valid region of γ_U (first assumption in Equation (17)). Overall, (22) involves subtracting a negative quantity from a positive, thus we have $\frac{\partial^2 C}{\partial \gamma_U^2} > 0$.

APPENDIX B PROOF OF THEOREM 1

C has four different "types" of Q-function terms in it as summands, with a total of $2\mathcal{K}$ separate Q-functions. By plugging in $\gamma_U = \gamma_U^*(\alpha_U)$ from (18), each of these Q-functions can be shown to be convex in α_U .

• Let $E_i = Q\left(\frac{B\alpha_U(h_1 - h_i)}{\sqrt{B\alpha_U(h_1 + h_i)}}\right)$: The convexity of this part follows from the fact that their derivative is an increasing function of α_U . Given the constraints in (17) are met,

$$\frac{\partial E_i}{\partial \alpha_U} = -\frac{B(h_1 - h_i)e^{-\frac{B\alpha_U(h_1 - h_i)^2}{2(h_1 + h_i)}}}{\sqrt{8\pi B\alpha_U(h_1 + h_i)}} = -K_1 \frac{e^{-k_1\alpha_U}}{\sqrt{\alpha_U}}$$
(23)

where K_1 and k_1 are positive coefficients. $e^{-k_1\alpha_U}$ is a decreasing function of α_U , whereas $\sqrt{\alpha_U}$ is an increasing function of it. The division of a decreasing and an increasing function is decreasing, and the minus sign makes the whole expression increasing.

- Let $F_i = Q\left(\frac{B(1-\alpha_U)(h_1-h_i)}{\sqrt{B(1-\alpha_U)(h_1+h_i)}}\right)$: The convexity of this part is proven in a very similar manner to E_i , by showing that $\frac{\partial F_i}{\partial \alpha_U}$ is an increasing function of α_U .
- Let $G=Q\left(\frac{B\alpha_Uh_1-\gamma_U}{\sqrt{B\alpha_Uh_1}}\right)$: The proof of this expression follows from its second derivative being always positive. The second derivative can be written as:

$$\frac{\partial^{2} G}{\partial \alpha_{U}^{2}} = \frac{e^{-\frac{(B\alpha_{U}h_{1} - \gamma_{U})^{2}}{2B\alpha_{U}h_{1}}}}{\sqrt{32\pi}\alpha_{U}^{2}(B\alpha_{U}h_{1})^{\frac{3}{2}}} \times \left(-\gamma_{U}^{3} - (B\alpha_{U}h_{1})\gamma_{U}^{2} + (B\alpha_{U}h_{1})^{3} + (B\alpha_{U}h_{1})^{2} + (B\alpha_{U}h_{1})^{2}\gamma_{U} + 3(B\alpha_{U}h_{1})\right). \tag{24}$$

The fraction in the first row of (24) is always positive, hence it is sufficient to show the positivity of the expression within the parentheses. Since the assumptions in (17) imply $\gamma_U < B\alpha_U h_1$, the inequalities $(B\alpha_U h_1)^3 > (B\alpha_U h_1)\gamma_U^2$ and $(B\alpha_U h_1)^2\gamma_U > \gamma_U^3$ hold and said expression is also guaranteed to be positive, making $\frac{\partial^2 G}{\partial \alpha_U^2} > 0$.

• Let $H=Q\left(\frac{B(1-\alpha_U)h_1-\gamma_U}{\sqrt{B(1-\alpha)h_1}}\right)$: Similar to G, the proof of this expression follows from $\frac{\partial^2 H}{\partial \alpha_U^2}>0$. Unfortunately, unlike the earlier Q-function types, H is not always convex in α_U for all valid γ_U . However, given the conditions in (17) are met, H is indeed convex in α_U when $\gamma_U=\gamma_U^*(\alpha_U)$. The second derivative evaluated at γ_U^* can be written as

$$\frac{\partial^{2} H}{\partial \alpha_{U}^{2}} = \frac{e^{-\frac{(\gamma_{U}^{*} - B\alpha_{U}h_{1})^{2}}{2B(1 - \alpha_{U})h_{1}}}}{(1 - \alpha_{U})^{2}(2\alpha_{U} - 1)\sqrt{32\pi B(1 - \alpha_{U})h_{1}}} \times \left[(1 - 2\alpha_{U}) \left(B^{2}h_{1}^{2}(2\alpha_{U}^{2} - 3\alpha_{U} + 1) + B(1 - \alpha_{U})h_{1} + Bh_{1}(1 - 2\alpha_{U})\gamma_{U}^{*} + 3\gamma_{U}^{*} \right) - \alpha_{U} \left(B(1 - \alpha_{U})h_{1} + \gamma_{U}^{*} \right) \ln\left(\frac{1 - \alpha_{U}}{\alpha_{U}}\right) \right].$$

Similar to G, the fraction in the first row of (25) is always positive. Thus, showing that the expression in the square brackets is positive is sufficient to ensure the convexity of H. Rearranging the terms, the positivity of the said part is guaranteed when the following inequality holds:

$$\gamma_U^* > B(1 - \alpha_U)h_1 \frac{1 - Bh_1(2\alpha_U - 1)}{Bh_1(2\alpha_U - 1) - 3}.$$
 (26)

By definition, $\gamma_U^* > B(1-\alpha_U)h_1$. Thus, ensuring $\frac{1-Bh_1(2\alpha_U-1)}{Bh_1(2\alpha_U-1)-3} \leq 1$ is sufficient for (26) to hold. This implies

-
$$B\alpha_U h_1 - B(1 - \alpha_U)h_1 > 3$$
, or
- $B\alpha_U h_1 - B(1 - \alpha_U)h_1 \le 2$,

where the former is within the assumption set in (17).

Lastly, since each summand in C is convex given the assumption set (17) is satisfied, the sum of these convex functions (i.e., C) is also convex.

REFERENCES

- M. C. Gursoy, D. Seo, and U. Mitra, "Concentration and position-based hybrid modulation scheme for molecular communications," in *IEEE Int. Conf. Commun. (ICC)*, Jun. 2020, pp. 1–6.
- [2] T. Suda, M. Moore, T. Nakano, R. Egashira, A. Enomoto, S. Hiyama, and Y. Moritani, "Exploratory research on molecular communication between nanomachines," in *Genet. Evol. Comput. Conf. (GECCO)*, Jun. 2005, pp. 25–29.
- [3] N. Farsad, H. B. Yilmaz, A. Eckford, C. B. Chae, and W. Guo, "A comprehensive survey of recent advancements in molecular communication," *IEEE Commun. Surveys Tutor.*, vol. 18, no. 3, pp. 1887–1919, Feb. 2016.
- [4] K. V. Srinivas, A. W. Eckford, and R. S. Adve, "Molecular communication in fluid media: The additive inverse Gaussian noise channel," *IEEE Trans. Info. Theory*, vol. 58, no. 7, pp. 4678–4692, July 2012.
- [5] M. Kuscu, E. Dinc, B. A. Bilgin, H. Ramezani, and O. B. Akan, "Transmitter and receiver architectures for molecular communications: A survey on physical design with modulation, coding, and detection techniques," *Proc. IEEE*, vol. 107, no. 7, pp. 1302–1341, Jul. 2019.
- [6] M. S. Kuran, H. B. Yilmaz, T. Tugcu, and I. F. Akyildiz, "Modulation techniques for communication via diffusion in nanonetworks," in *Proc. IEEE Int. Conf. Commun. (ICC)*, Apr. 2011, pp. 1–5.
- [7] N.-R. Kim and C.-B. Chae, "Novel modulation techniques using isomers as messenger molecules for nano communication networks via diffusion," *IEEE J. Sel. Areas Commun.*, vol. 31, no. 12, pp. 847–856, Jan. 2013.
- [8] N. Garralda, I. Llatser, A. Cabellos-Aparicio, E. Alarcón, and M. Pierobon, "Diffusion-based physical channel identification in molecular nanonetworks," *Nano Commun. Netw.*, vol. 2, no. 4, pp. 196–204, Dec. 2011.
- [9] H. Arjmandi, A. Gohari, M. N. Kenari, and F. Bateni, "Diffusion-based nanonetworking: A new modulation technique and performance analysis," *IEEE Commun. Lett.*, vol. 17, no. 4, pp. 645–648, Mar. 2013.
- [10] M. H. Kabir, S. M. R. Islam, and K. S. Kwak, "D-MoSK modulation in molecular communications," *IEEE Trans. Nanobiosci.*, vol. 14, no. 6, pp. 680–683, Sep. 2015.
- [11] S. Pudasaini, S. Shin, and K. S. Kwak, "Robust modulation technique for diffusion-based molecular communication in nanonetworks," arXiv preprint arXiv:1401.3938, 2014.
- [12] B. Tepekule, A. E. Pusane, H. B. Yilmaz, C.-B. Chae, and T. Tugcu, "ISI mitigation techniques in molecular communication," *IEEE Trans. Mol. Biol. Multi-Scale Commun.*, vol. 1, no. 2, pp. 202–216, Jun. 2015.
- [13] S. Pudasaini, S. Shin, and K. S. Kwak, "Run-length aware hybrid modulation scheme for diffusion-based molecular communication," in *Proc. IEEE Int. Symp. on Commun. Info. Tech. (ISCIT)*, Sept. 2014, pp. 439–442.
- [14] S. Sharma, K. Deka, and V. Bhatia, "Hybrid modulation scheme and modified energy detector for molecular communications," in *IEEE Int. Conf. on Adv. Netw. Telecommun. Sys. (ANTS)*, Dec. 2019, pp. 1–4.
- [15] I. Oppermann, M. Hämäläinen, and J. Iinatti, UWB: theory and applications. John Wiley & Sons, 2005.
- [16] P. H. Pathak, X. Feng, P. Hu, and P. Mohapatra, "Visible light communication, networking, and sensing: A survey, potential and challenges," *IEEE Commun. Surveys Tutor.*, vol. 17, no. 4, pp. 2047–2077, Sep. 2015.
- [17] Y. Murin, N. Farsad, M. Chowdhury, and A. Goldsmith, "Optimal detection for one-shot transmission over diffusion-based molecular timing channels," *IEEE Trans. Mol. Biol. Multi-Scale Commun.*, vol. 4, no. 2, pp. 43–60, Jun. 2018.
- [18] B. C. Akdeniz, A. E. Pusane, and T. Tugcu, "Position-based modulation in molecular communications," *Nano Commun. Netw.*, vol. 16, pp. 60– 68, Jun. 2018.
- [19] F. Mirkarimi, M. Mirmohseni, and M. Nasiri-Kenari, "On the capacity of the joint time and concentration modulation for molecular communications," arXiv preprint arXiv:2006.13398, Jun. 2020.

- [20] H. B. Yilmaz, A. C. Heren, T. Tugcu, and C.-B. Chae, "Three-dimensional channel characteristics for molecular communications with an absorbing receiver," *IEEE Commun. Lett.*, vol. 18, no. 6, pp. 929–932, Jun. 2014.
- [21] G. Aminian, H. Arjmandi, A. Gohari, M. Nasiri-Kenari, and U. Mitra, "Capacity of diffusion-based molecular communication networks over LTI-Poisson channels," *IEEE Trans. Mol. Biol. Multi-Scale Commun.*, vol. 1, no. 2, pp. 188–201, Nov. 2015.
- [22] M. Ş. Kuran, H. B. Yilmaz, T. Tugcu, and B. Özerman, "Energy model for communication via diffusion in nanonetworks," *Nano Commun. Netw.*, vol. 1, no. 2, pp. 86–95, Jun. 2010.
- [23] D. Kilinc and O. B. Akan, "Receiver design for molecular communication," *IEEE J. Sel. Areas Commun.*, vol. 31, no. 12, pp. 705–714, Dec. 2013.
- [24] A. Viterbi, "Error bounds for convolutional codes and an asymptotically optimum decoding algorithm," *IEEE Trans. Info. Theory*, vol. 13, no. 2, pp. 260–269, Apr. 1967.
- [25] V. Jamali, A. Ahmadzadeh, and R. Schober, "On the design of matched filters for molecule counting receivers," *IEEE Commun. Lett.*, vol. 21, no. 8, pp. 1711–1714, May 2017.
- [26] H. B. Yilmaz and C.-B. Chae, "Arrival modelling for molecular communication via diffusion," *IET Elec. Lett.*, Nov. 2014.
- [27] M. C. Gursoy, B. C. Akdeniz, T. Tugcu, and A. E. Pusane, "Error probability calculation with reduced complexity for molecular communications," in *Int. Conf. Telecommun. Sig. Proc. (TSP)*, Jul. 2018, pp. 1–4.
- [28] J. J. Kim and K. Park, "Modulated insulin delivery from glucosesensitive hydrogel dosage forms," *Journal of Controlled Release*, vol. 77, no. 1-2, pp. 39–47, Nov. 2001.
- [29] A. F. Molisch, Wireless communications. John Wiley & Sons, 2012.
- [30] T. Tung and U. Mitra, "Synchronization error robust transceivers for molecular communication," *IEEE Trans. Mol. Biol. Multi-Scale Commun.*, vol. 5, no. 3, pp. 207–221, Dec. 2019.
- [31] B. C. Akdeniz, A. E. Pusane, and T. Tugcu, "Optimal reception delay in diffusion-based molecular communication," *IEEE Commun. Lett.*, vol. 22, no. 1, pp. 57–60, Jan. 2018.



Daewon Seo received the B.S. and M.S. degrees in electrical engineering from the Korea Advanced Institute of Science and Technology, Daejeon, South Korea, in 2008 and 2010, respectively, and the Ph.D. degree in electrical and computer engineering from the University of Illinois at Urbana-Champaign in 2019. He is currently a postdoctoral researcher with the department of electrical and computer engineering, the University of Wisconsin-Madison, Madison, WI, USA. He was with KAIST Institute and LG Electronics, South Korea, from 2010 to 2011 and

from 2011 to 2014, respectively. He was with the University of Southern California, Los Angeles, CA, USA, in 2019 as a postdoctoral researcher. His research interests include machine learning theory, information theory, and statistical signal processing.

Urbashi Mitra received the B.S. and the M.S. degrees from the University of California at Berkeley and her Ph.D. from Princeton University. She is currently the Gordon S. Marshall Professor in Engineering at the University of Southern California with appointments in Electrical Engineering and Computer Science. She is the inaugural Editor-in-Chief for the IEEE Transactions on Molecular, Biological and Multi-scale Communications. She was a member of the IEEE Information Theory Society's Board of Governors (2002-2007, 2012-2017), the IEEE Signal Processing Society's Technical Committee on Signal Processing for Communications and Networks (2012-2017), the IEEE Signal Processing Society's Awards Board (2017-2018), and the Vice Chair of the IEEE Communications Society, Communication Theory Working Group (2017-2018). Dr. Mitra is a Fellow of the IEEE. She is the recipient of: the 2017 IEEE Communications Society Women in Communications Engineering Technical Achievement Award, a 2016 UK Royal Academy of Engineering Distinguished Visiting Professorship, a 2016 US Fulbright Scholar Award, a 2016-2017 UK Leverhulme Trust Visiting Professorship, 2015-2016 IEEE Communications Society Distinguished Lecturer, 2012 Globecom Signal Processing for Communications Symposium Best Paper Award, 2012 US National Academy of Engineering Lillian Gilbreth Lectureship, the 2009 DCOSS Applications & Systems Best Paper Award, Texas Instruments Visiting Professor (Fall 2002, Rice University), 2001 Okawa Foundation Award, 2000 OSU College of Engineering Lumley Award for Research, 1997 OSU College of Engineering MacQuigg Award for Teaching, and a 1996 National Science Foundation CAREER Award. Her research interests are in: wireless communications, communication and sensor networks, biological communication systems, detection and estimation and the interface of communication, sensing and control.



Mustafa Can Gursoy received the B.S. and M.S. degrees in electrical and electronics engineering from Bogazici University, Istanbul, Turkey, in 2015 and 2017, respectively. He is currently a Ph.D. student and a research assistant working at Ming Hsieh Department of Electrical and Computer Engineering, University of Southern California, Los Angeles, USA. His research interests include transceiver design, channel modeling, and networking approaches for molecular communications.